ARTICLE

Preparation and Electrochemical Performance of V_2O_3-C Dual-Layer Coated $LiFePO_4$ by Carbothermic Reduction of V_2O_5

You-liang Wei, Hong-fa Xiang*

School of Materials Science and Engineering, Hefei University of Technology, Hefei 230009, China

(Dated: Received on February 20, 2015; Accepted on April 10, 2015)

The V_2O_3-C dual-layer coated $LiFePO_4$ cathode materials with excellent rate capability and cycling stability were prepared by carbothermic reduction of V_2O_5. X-ray powder diffraction, elemental analyzer, high resolution transmission electron microscopy and Raman spectra revealed that the V_2O_3 phase co-existed with carbon in the coating layer of $LiFePO_4$ particles and the carbon content reduced without graphitization degree changing after the carbothermic reduction of V_2O_5. The electrochemical measurement results indicated that small amounts of V_2O_3 improved rate capability and cycling stability at elevated temperature of $LiFePO_4$/C cathode materials. The V_2O_3-C dual-layer coated $LiFePO_4$ composite with 1wt% vanadium oxide delivered an initial specific capacity of 167 mAh/g at 0.2 C and 129 mAh/g at 5 C as well as excellent cycling stability. Even at elevated temperature of 55 °C, the specific capacity of 151 mAh/g was achieved at 1 C without capacity fading after 100 cycles.

Key words: Lithium iron phosphate, Vanadium oxide, Carbon coating, Li-ion battery

I. INTRODUCTION

$LiFePO_4$ has attracted extensive attention as cathode material for the large-sized lithium-ion batteries in application of electric vehicles (EVs) and the energy storage systems, owing to its excellent safety and long lifespan [1]. In the last work, huge advances have been made to improve intrinsically poor electronic conductivity and slow Li^+ extraction-insertion kinetics, including surface coating or admixing with electronically conductive materials [2–6], reducing particle size to nanoscale and controlling morphology [7–11], and doping with supervalent cations [12–16]. Nanostructure design can shorten Li^+ transport distance and bulk doping is an effective way to expand the lattice paths, both of which can facilitate the Li^+ insertion-extraction kinetics. Surface coating is an indispensable technique in commercial products, in order to enhance the electronic conductivity of $LiFePO_4$.

Coating a conducting component, such as carbon, metals or conducting polymers on the particle surface is very effective to improve the electronic conductivity of $LiFePO_4$. Among them, carbon coating is particularly attractive due to its high conductivity, low cost for sources and preparation technology, and excellent chemical stability in the battery. On one hand, a homogeneous coated carbon layer can definitely improve the electronic conductivity between the $LiFePO_4$ particles. On the other hand, the rigorous carbon layer can effectively suppress the particles agglomeration during the solid-state preparation of $LiFePO_4$ [17]. Both these two points require a thick carbon layer coating, inevitably along with a compromise to volumetric energy density [18]. A combination of carbon coating and particle refinement for $LiFePO_4$ has been commercialized in the state-of-the-art battery industry. Many researches focus on carbon coating on $LiFePO_4$ particles by firing one carbon source (organic or polymeric compounds) during or after the $LiFePO_4$ synthesis [2–5]. However, it is difficult to meet the rigorous requirement of applications in EVs and smart grids by simple carbon coating. Recently, introduction of the second phase has been proven a promising route to satisfy the development of $LiFePO_4$. Oh *et al.* reported a double carbon coating on microscale nanoporous $LiFePO_4$ to improve the uniformity of carbon coating combining with high tap density [4]. Carbon coated $FePO_4$ was first prepared by using sucrose as the first carbon source, and finally the $LiFePO_4$/C microspheres containing about 0.5wt% carbon with a high tap density of 1.5 g/cm^3 were synthesized by using pitch as the second carbon source. Other non-carbon second phase (*e.g.* metal oxides, polymers) coatings were widely reported to modify the $LiFePO_4$ surface [19–22]. Metal oxide has been used to improve the performance of $LiFePO_4$. It was also found that CeO_2, ZrO_2 and TiO_2 can not only enhance the electrochemical performance but also improve the thermal stability. The metal oxide layer functioned as a protecting layer against HF was attacked from the

*Author to whom correspondence should be addressed. E-mail: hfxiang@hfut.edu.cn, Tel.: +86-551-62901457, FAX: +86-551-62901362

electrolyte [23]. As a result, ferrous dissolution in the electrolyte can be effectively suppressed, and thus the electrochemical performance of $LiFePO_4$, especially the cycling lifetime, was enhanced at both room temperature and elevated temperature.

Most recently, vanadium oxides have become one of the most attractive candidates as surface coating material for various cathode materials [24–27]. V_2O_5 and VO_x have been extensively investigated as a protective surface layer on $LiCoO_2$, $LiNiO_2$, $LiNi_{1/3}Co_{1/3}Mn_{1/3}O_2$, and $Li_{1.2}Ni_{0.16}Co_{0.08}Mn_{0.56}O_2$ particles against side reactions with the electrolyte and the cations dissolution into the electrolyte. However, just similar to most metal oxides, the low electronic conductivity of V_2O_5 results in its failure as the surface layer of $LiFePO_4$ particles. It is interesting to recognize that V_2O_3 exhibits quasi-metallic conductivity of over 10^{-3} S/cm at room temperature, which is even higher than V_2O_5 by 6−7 orders of magnitude [28–31]. Recently, Jin *et al.* used ammonium metavanadate as the vanadium source to synthesize V_2O_3-modified $LiFePO_4$/C materials via a one-step solid-state process [32]. The V_2O_3-modified $LiFePO_4$/C materials exhibit improved rate and low-temperature performance. However, during the one-step process, the adjustment on the C-V_2O_3 coating layer on the $LiFePO_4$ particles is still a big challenge.

In this work, we attempt to develop a novel approach for V_2O_3-C dual-layer coating on $LiFePO_4$ by carbothermic reduction of V_2O_5. As illustrated in Fig.1, a thick carbon layer on the carbon-coated $LiFePO_4$ composite is facile to form a uniform coating and also effectively limit the growth of $LiFePO_4$ particles. But the high content of carbon will significantly reduce the tap density of the $LiFePO_4$/C composite and thus cause the energy density of the related batteries. Herein, V_2O_3 as the second phase is introduced into the $LiFePO_4$ composite by the carbothermic reduction of V_2O_5 ($2C+V_2O_5 \rightarrow V_2O_3+2CO$). During the carbothermic reduction process of V_2O_5, partial carbon is transferred into CO gas so that the resulting thin carbon layer is helpful to achieve the high tap density of $LiFePO_4$ materials. In addition, V_2O_3 is expected to give more efficient protection on $LiFePO_4$ against the electrolyte without reducing the electronic conductivity so that the cycling stability of $LiFePO_4$ at elevated temperature can be improved.

II. EXPERIMENTS

A. Synthesis of V_2O_3-C coated $LiFePO_4$

Firstly, $LiFePO_4$/C composite was prepared by a simple solid-state reaction. A mixture of ferrous oxalate hydrate ($FeC_2O_4{\cdot}2H_2O$), ammonium dihydrogen phosphate ($NH_4H_2PO_4$) and lithium carbonate (Li_2CO_3) in a stoichiometric molar ratio (1:1:0.53) was grounded in cyclohexane for 8 h by wet ball-milling at the rate of 300 r/min. After being dried at 80 °C, the mixture was heated at 350 °C for 6 h under N_2 atmosphere to obtain the intermediate powders. Then, the intermediate was mixed with polyvinyl alcohol (PVA, as carbon source) and milled for 4 h under the same conditions as above. Here, the weight of PVA was 20wt% of the final $LiFePO_4$. After the milling and dry, the collected powders were subsequently sintered at 700 °C for 5 h under N_2 atmosphere to get the $LiFePO_4$/C composite. In order to achieve V_2O_3-C dual-layer coating, the $LiFePO_4$/C composite was mixed with different amounts of V_2O_5. After 4 h milling and 5 h sintering, the V_2O_3-C dual-layer coated $LiFePO_4$ composites were obtained through the carbothermic reduction of V_2O_5. The obtained V_2O_3-C coated $LiFePO_4$ composites were named as V0, V1, and V5, corresponding to 0wt%, 1wt%, and 5wt% V_2O_5 addition, respectively.

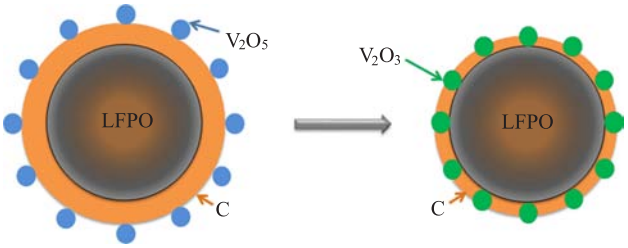

FIG. 1 Schematic illustration for the formation of the V_2O_3-C dual-layer coated on the $LiFePO_4$ particles by carbothermic reduction of V_2O_5.

B. Characterization and electrochemical measurements

The crystal structures of the V_2O_3-C coated $LiFePO_4$ composites were identified by X-ray diffraction (XRD) measurements (D/max2500V) using Cu Kα (λ=1.5406 Å) radiation in 2θ range of 10°−60°. The amount of carbon in the samples was estimated using an elemental analyzer (Vario EL c). Raman spectra were obtained on a Raman spectrometer employing a 10 mW helium/neon laser with a wavelength of 632.8 nm. The morphologies of the $LiFePO_4$ composites were investigated by high resolution transmission electron microscopy (HRTEM) (JEM-2100F).

In order to make the electrode laminate for the electrochemical measurements, a slurry containing 80wt% samples as active material, 10wt% super P and 10wt% polyvinylidene fluoride (PVDF) dispersed in *N*-methyl-2-pyrrolidinone (NMP) was cast onto an aluminum current collector. After vacuum drying at 80 °C, the laminate was punched into discs (Φ14 mm) for assembling the CR2032-type coin cells. The mass loading in the electrode was controlled at about 6 mg/cm^2. Celgard 2400 microporous polypropylene membrane was used as separator. The electrolyte was 1 mol/L $LiPF_6$ in a mixture of ethylene carbonate (EC) and diethyl carbonate

DOI:10.1063/1674-0068/28/cjcp1502025

(DEC) (1:1 mass ratio). The cells were assembled in an Ar-filled glove box (MBraun) using highly pure lithium foil as the counter and reference electrode.

All the cells were galvanostatically charged and discharged in the range of 4.2−2.0 V at 0.2 C (1 C=170 mAh/g) for the two formation cycles on a multichannel battery cycler (Neware BTS2300, Shenzhen) at room temperature. Then the cycling tests were performed at a current rate of 1 C. For the high temperature tests, the cells were cycled at 55 °C in an oven. To evaluate the rate capability, the cells were charged to 4.2 V at 0.2 C and discharged to 2.0 V at various rates. Electrochemical impedance spectroscopy (EIS) of the cells was performed on a CHI 604D electrochemistry workstation (Shanghai Chenhua Instruments Co. Ltd.) with the frequency range and potential perturbation set as 100 kHz to 10 mHz and 10 mV, respectively.

III. RESULTS AND DISCUSSION

A. Structure and morphology

Figure 2 shows the XRD patterns and the carbon contents of the V_2O_3-C coated $LiFePO_4$ composites. From Fig.2(a), it is obvious that the main phase in these composites is orthorhombic olivine $LiFePO_4$ with a space group of *Pmnb*. Besides the peaks of $LiFePO_4$, the main diffraction peaks corresponding to (104), (110), (113) and (116) planes of V_2O_3 and (310) plane of V_2O_5 are clearly detected in V5. The formation of V_2O_3 is resulted from the carbothermic reduction of V_2O_5. With the addition of 5wt% V_2O_5, the carbothermic reduction is not performed completely so that still some V_2O_5 residues existed in V5. In V1, no any diffraction peak was shown owing to the low contents (<1wt%) of vanadium oxides, just similar to the ZrO_2, SiO_2 and CuO-coated $LiFePO_4$/C composites [20, 33, 34]. Carbon in all the composites was amorphous and no diffiraction peak was detected. Figure 2(b) shows the carbon contents in the composites by elemental analysis. Because of the carbon consumption during the carbothermic reduction of V_2O_5, the carbon content decreases with increasing the content of vanadium. The carbon contents in V0, V1, and V5 are 6.3wt%, 3.8wt% and 2.4wt%, respectively. It is interesting that the carbothermic reduction of 1wt% V_2O_5 resulted in a striking difference of 2.5% (6.3%−3.8%), but introduction of another 4wt% V_2O_5 only caused a slight reduction of 1.4wt% (3.8wt%−2.4wt%) in the carbon content. This result suggests that the carbothermic reduction of V_2O_5 in V5 is not thoroughgoing, which is consistent with the XRD results.

To further determine the surface structure of the V_2O_3-C $LiFePO_4$ composites, we observe these composites by HRTEM (Fig.3). As shown in Fig.3(a), a carbon layer with the thickness of ∼4 nm was coated on the surface of $LiFePO_4$ particle in V0. This carbon was amorphous and uniform. However, after the carbothermic reduction of V_2O_5 in V1 and V5 (Fig.3 (b) and (c)), the surface layer on the $LiFePO_4$ particles became quite complicated, and some clear lattice fringes were observed in the surface layer. After calculating the plane spacing, we can confirm that some V_2O_3 grains exist in the surface coating layers of V1 and V5. Hence, the surface of $LiFePO_4$ particles in V1 and V5 is actually modified by V_2O_3 grains that are embedded in an amorphous carbon layer.

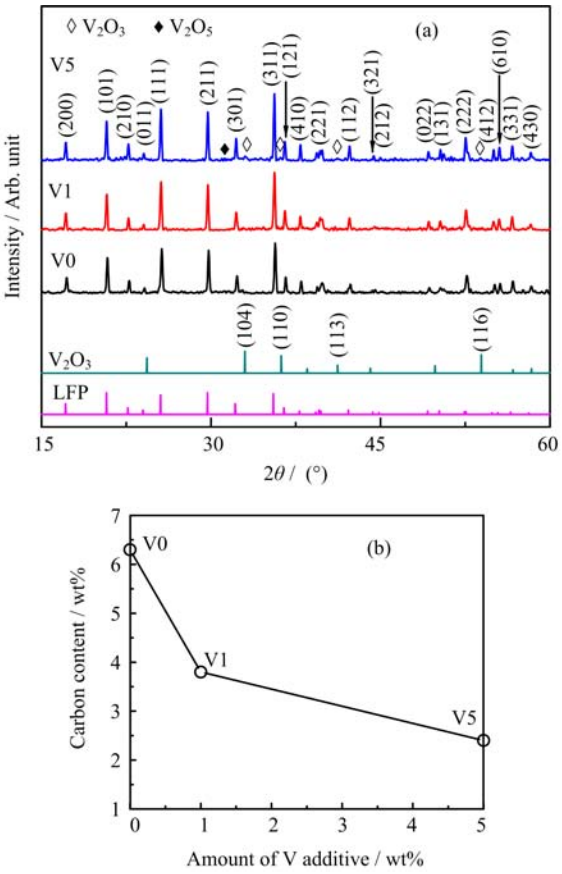

FIG. 2 (a) XRD pattern of the V_2O_3-C dual-layer coated on the $LiFePO_4$ nanoparticles and (b) the relationship of carbon content *vs.* vanadium oxide content.

Jin *et al.* claimed that the presence of vanadium oxide can increase the degree of graphitization in the $LiFePO_4$/C composite [32]. Raman spectrum is an effective method to detect the graphitization degree of the carbon component. As shown in Fig.4, each spectrum consists of two broad peaks at 1350 and 1600 cm^{-1}, corresponding to the D-band and G-band, respectively. G-band is a typical character of graphitic carbon, but D-band is usually related to the defects, edge sites and pores [35, 36]. According to previous literatures [37, 38], these two peaks can be fitted with four separated dotted-line peaks at 1194, 1347, 1510, and 1585 cm^{-1}, respectively. The peaks at 1347 and 1585 cm^{-1} are contributed to sp^2-type carbon, while

DOI:10.1063/1674-0068/28/cjcp1502025

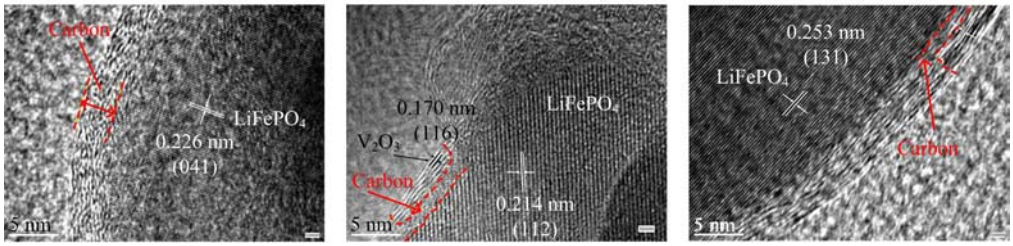

FIG. 3 HRTEM images of (a) V0, (b) V1, and (c) V5.

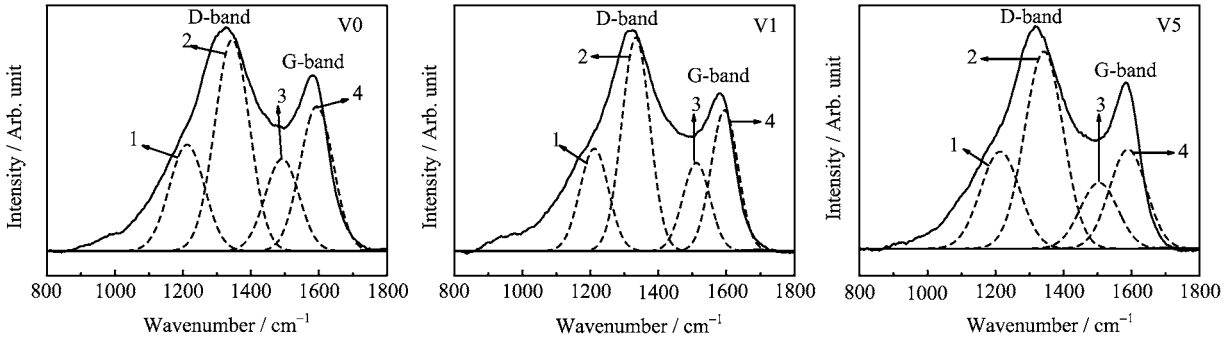

FIG. 4 Raman spectra of V0, V1, and V5. 1: 1194 cm^{-1}, 2: 1347 cm^{-1}, 3: 1510 cm^{-1}, 4: 1585 cm^{-1}.

the peaks at 1194 and 1510 cm^{-1} reflect to sp^3-type carbon. Herein, the degree of graphitization of carbon can be calculated by the integrated intensity ratio I_{sp^2}/I_{sp^3}, where I_{sp^2} and I_{sp^3} are the total areas of the sp^2-type peaks (1347 and 1585 cm^{-1}) and the sp^3-type peaks (1194 and 1510 cm^{-1}). Herein, the I_{sp^2}/I_{sp^3} values of V0, V1 and V5 are 1.76, 1.78 and 1.79, respectively. Therefore, it is concluded that the graphitization degree of the carbon component did not change during the carbothermic reduction of V_2O_5.

B. Electrochemical performance

Figure 5 shows typical initial charge-discharge voltage profiles of V_2O_3-C coated $LiFePO_4$ composites. The tests were performed galvanostatically at 0.2 C in the range 2.0−4.2 V. The charge-discharge voltage profiles appeared with the typical voltage plateau (at 3.45 V *vs.* Li^+/Li), which is attributed to the two-phase reaction of the $(1-x)FePO_4+xLiFePO_4$ system. The initial discharge capacities of V0, V1, and V5 are 147, 167, and 162 mAh/g, respectively. The V_2O_3-C coated $LiFePO_4$ composites (V1 and V5) exhibited a higher reversible capacity than the pristine $LiFePO_4$/C composite (V0). Especially for V1, its initial capacity of 167 mAh/g at 0.2 C is over 98.6% of the theoretical capacity of $LiFePO_4$. In addition, the charge and discharge voltage plateaus of V0 and V1 are very close. But V5 has the slightly lower discharge voltage plateau than the others. The gap between charge and discharge voltage plateaus,

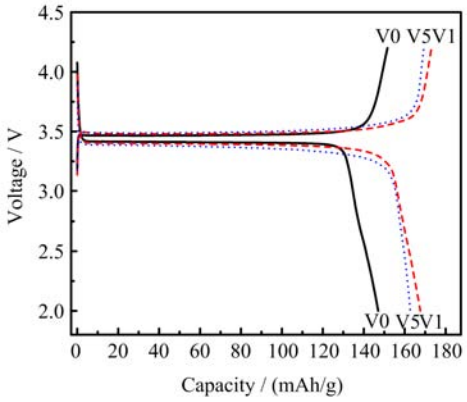

FIG. 5 Initial charge and discharge capacities of the cells using V0, V1, and V5 at 0.2 C.

which is one of the indicators of polarization, of V5 is bigger than that of V1. The high polarization of V5 is possibly attributed to the existence of non-conductive V_2O_5.

In order to further explain the difference of the electrochemical behaviors between V0, V1 and V5, electrochemical impedance spectra were carried out after the initial cycle (Fig.6). All impedance curves include a semicircle in high-to-medium frequency region and an inclined line in low frequency region. The semicircle is due to the charge transfer impedance and the inclined line is considered as Warburg impedance, which repre-

DOI:10.1063/1674-0068/28/cjcp1502025

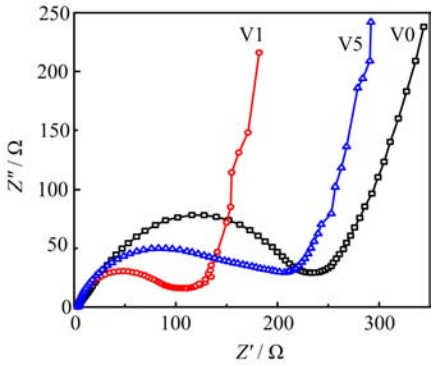

FIG. 6 Nyquist plots of the cells using V0, V1, and V5 after the initial cycle.

sents lithium-ion diffusion process. Here it is clear that V1 has the lowest charge transfer impedance among three composites, indicating the fast transfer rate of Li ions and electrons in V1. The contributions of electron conduction and lithium transport from the V_2O_3-C dual-layer promote together the excellent electrochemical performance of V1.

The cycling performance of V0, V1, and V5 at room temperature and elevated temperature is shown in Fig.7. Figure 7(a) shows the cycling behaviors of these three samples at 25 °C at 1 C. At the first cycle after the two formation cycles, the discharge capacities of V0, V1, and V5 are 129, 152 and 143 mAh/g, respectively. After 100 cycles, V0 and V1 have similarly negligible capacity fading, but V5 exhibits a gradual capacity drop from the initial 143 mAh/g to 117 mAh/g. Therefore, the coating layer in V5 composed of too much vanadium oxides (5wt%), especially including V_2O_5, is not stable enough to long-term charge-discharge cycling. However, V0 and V1 both have the excellent cycling stability, and the V_2O_3-C dual-layer coated $LiFePO_4$ composite delivers the higher capacity than V0 at 1 C at room temperature. The cycling stabilities of V0 and V1 at elevated temperature (55 °C) at 1 C are further compared in Fig.7(b). The initial discharge capacities of V0 and V1 are 151 and 158 mAh/g. During 100 cycles, V1 has no capacity fading, but V0 exhibits a gradual capacity drop after the 80th cycle. According to previous studies [39, 40], it is a common problem that the $LiFePO_4$/C cathode material has capacity attenuation at elevated temperature. The main reason is that the decomposition of materials and side reactions would occur at electrode/electrolyte interface [41]. The reaction between $LiFePO_4$ and the electrolyte made a part of Fe^{2+} ions dissolve into the electrolyte, which resulted in the cycling fading of $LiFePO_4$/C (V0). Basically, it is concluded that the coating of vanadium oxide in V1 can suppress the Fe^{2+} dissolution and improve the cycling stability of $LiFePO_4$ at elevated temperature.

The discharge profiles of $LiFePO_4$/C and V_2O_3-C dual-layer coated $LiFePO_4$ composites at different rates

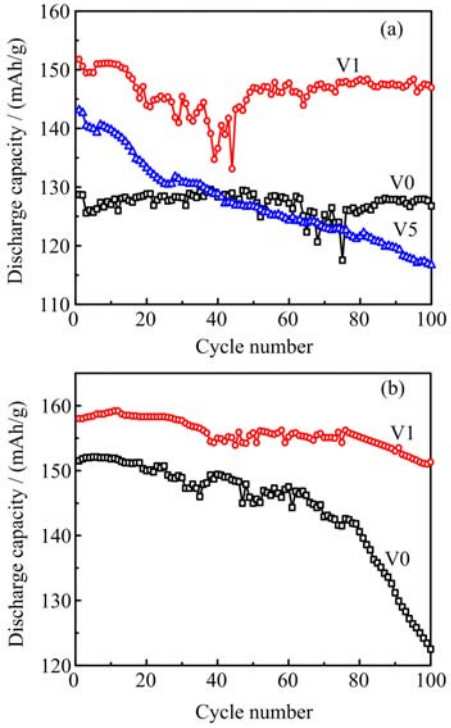

FIG. 7 Cycling performance of the cells using V0, V1 and V5 at 1 C at (a) 25 °C and (b) 55 °C.

are shown in Fig.8. All the cells using V0, V1 and V5 as cathode material were charged at the same current of 34 mAh/g (corresponding to 0.2 C rate) to ensure identical initial conditions for each discharge and then discharged at progressively increasing rates from 0.2 C (34 mAh/g) to 5 C (850 mAh/g). The electrode polarization becomes larger with the increase of current rate due to the limitation of electrochemical kinetics (Fig.8 (a)−(c)). Among the three $LiFePO_4$ composites, V1 displays the best rate performance, with the discharge capacities of about 167, 161, 156, 147 and 129 mAh/g at 0.2, 0.5, 1, 2, and 5 C, respectively. From Fig.8(d), it is distinct that V1 exhibits the highest discharge capacity at all rates. However, the discharge capacity decreases sharply for V5, especially at the high rate of 5 C. The high-rate discharge performance and excellent cycling stability of V1 indicated that the V_2O_3-C dual-layer coating improves surface electronic conductivity of $LiFePO_4$ particles and decreases the thickness of surface carbon layer, resulting in the excellent rate performance and cycling stability at elevated temperature.

IV. CONCLUSION

In this study, the V_2O_3 second phase was successfully impregnated into the surface carbon layer of the $LiFePO_4$/C cathode and the carbon content reduced without graphitization degree changing by carbothermic reduction of V_2O_5. The comparing study on the

DOI:10.1063/1674-0068/28/cjcp1502025

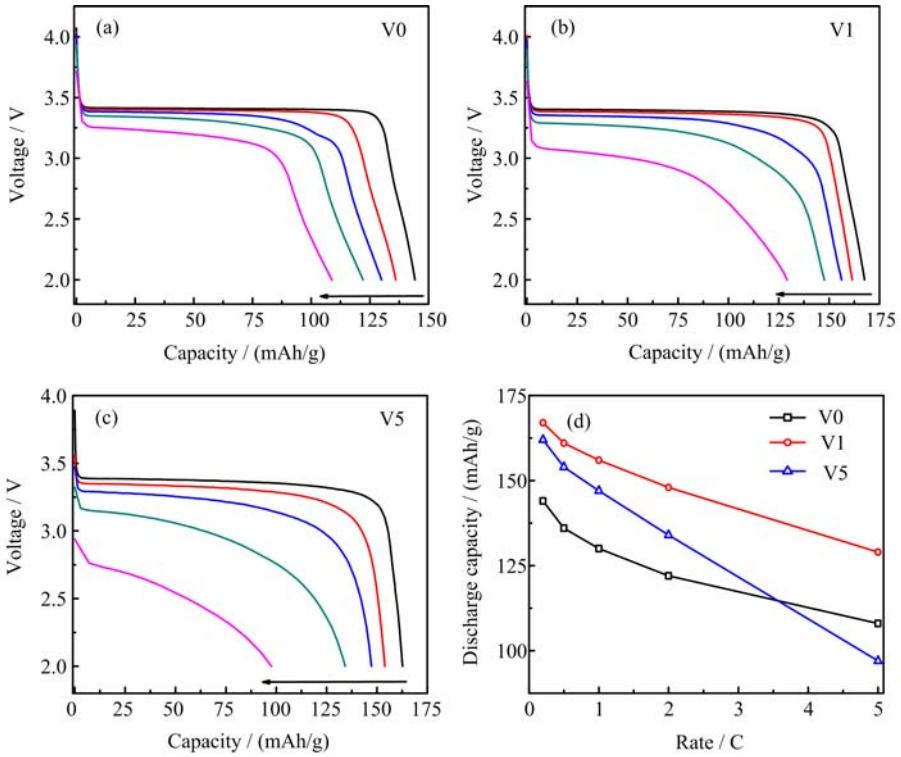

FIG. 8 Rate discharge curves of the cells using (a) V0, (b) V1, and (c) V5 at 0.2, 0.5, 1, 2, 5 C rates, as arrows show. (d) Discharge capacity values.

electrochemical performance of the V_2O_3-C dual-layer coated $LiFePO_4$ and the pristine $LiFePO_4$/C composites indicates that small amounts of V_2O_3 significantly improved rate capability and cycling stability at elevated temperature of $LiFePO_4$/C cathode materials in lithium ion batteries. The V_2O_3-C dual-layer coated $LiFePO_4$ with 1 wt% vanadium oxide shows excellent electrochemical performances with initial specific capacity of 167 mAh/g at 0.2 C and the specific capacity of 151 mAh/g at 1 C maintains no fading after 100 cycles at 55 °C. The dual-layer coating of carbon and V_2O_3 by the carbothermic reduction of V_2O_5 on the $LiFePO_4$ particles can not only improve the electronic conductivity, but also suppress the dissolution of Fe^{2+} and improve its cycling stability at elevated temperature. In addition, this coating approach is facile to reduce the coated carbon content without the compromise on the conductivity and particles agglomeration, which is very attractive to increase the energy density of the state-of-the-art $LiFePO_4$ batteries.

V. ACKNOWLEDGMENTS

This work was supported by the National Natural Science Foundation of China (No.21006033 and No.51372060) and the Fundamental Research Funds for the Central Universities (No.2013HGCH0002).

[1] B. Scrosati and J. Garche, J. Power Sources **195**, 2419 (2010).
[2] X. Y. Wu, L. Y. Jiang, F. F. Cao, Y. G. Guo, and L. J. Wan, Adv. Mater. **21**, 2710 (2009).
[3] G. Wang, H. Liu, J. Liu, S. Qiao, G. M. Lu, P. Munroe, and H. Ahn, Adv. Mater. **22**, 4944 (2010).
[4] S. W. Oh, S. T. Myung, S. M. Oh, K. H. Oh, K. Amine, B. Scrosati, and Y. K. Sun, Adv. Mater. **22**, 4842 (2010).
[5] Y. G. Huang, F. H. Zheng, X. H. Zhang, Q. Y. Li, and H. Q. Wang, Electrochim. Acta **130**, 740 (2014).
[6] Y. H. Huang, K. S. Park, and J. B. Goodenough, J. Electrochem. Soc. **153**, A2282 (2006).
[7] A. Yamada, S. C. Chung, and K. Hinokuma, J. Electrochem. Soc. **148**, A224 (2001).
[8] M. Takahashi, S. Tobishima, K. Takei, and Y. Sakurai, J. Power Sources **97**, 508 (2001).
[9] S. Franger, F. L. Cras, and C. Bourbon, J. Power Sources **119**, 252 (2003).
[10] X. H. Liu, J. Q. Wang, J. Y. Zhang, and S. R. Yang, J. Chem. Phys. **19**, 530 (2006).
[11] G. L. Huang, W. Li, H. Z. Sun, J. W. Wang, J. P. Zhang, H. X. Jiang, and F. Zhai, Electrochim. Acta **97**, 92 (2013).
[12] N. Ravet, A. Abouimrane, and M. Armand, Nat. Mater. **2**, 702 (2003).
[13] S. Y. Chung, J. T. Bloking, and Y. M. Chiang, Nat. Mater. **1**, 123 (2002).

DOI:10.1063/1674-0068/28/cjcp1502025

[14] P. S. Herle, B. Ellis, N. Coombs, and L. F. Nazar, Nat. Mater. **3**, 147 (2004).
[15] J. Hong, X. L. Wang, and Q. Wang, J. Phys. Chem. C **116**, 20787 (2012).
[16] L. L. Zhang, G. Liang, A. Ignatov, M. C. Croft, X. Q. Xiong, I. M. Hung, Y. H. Huang, X. L. Hu, W. X. Zhang, and Y. L. Peng, J. Phys. Chem. C **115**, 13520 (2011).
[17] P. P. Prosini, D. Zane, and M. Pasquali, Electrochim. Acta **46**, 3517 (2001).
[18] Z. Chen and J. R. Dahn, J. Electrochem. Soc. **149**, A1184 (2002).
[19] H. H. Chang, C. C. Chang, C. Y. Su, H. C. Wu, M. H. Yang, and N. L. Wu, J. Power Sources **185**, 466 (2008).
[20] H. Liu, G. X. Wang, D. Wexler, J. Z. Wang, and H. K. Liu, Electrochem. Commun. **10**, 165 (2008).
[21] D. Lepage, C. Michot, G. Liang, M. Gauthier, and S. B. Schougaard, Angew. Chem. Int. Ed. **50**, 6884 (2011).
[22] Y. H. Huang and J. B. Goodenough, Chem. Mater. **20**, 7237 (2008).
[23] Z. Chen, Y. Qin, K. Amine, and Y. K. Sun, J. Mater. Chem. **20**, 7606 (2010).
[24] J. W. Lee, S. M. Park, and H. J. Kim, J. Power Sources **188**, 583 (2009).
[25] X. Xiong, Z. Wang, and G. Yan, J. Power Sources **245**, 183 (2014).
[26] X. Liu, P. He, H. Li, M. Ishida, and H. Zhou, J. Alloys Compd. **552**, 76 (2013).
[27] K. S. Park, A. Benayad, and M. S. Park, Chem. Commun. **46**, 4190 (2010).
[28] X. Pan, G. F. Ren, M. N. F. Hoque, S. Bayne, K. Zhu, and Z. Y. Fan, Adv. Mater. Interfaces **1**, 1400398 (2014).
[29] Z. J. Lao, K. Konstantinov, Y. Tournaire, S. H. Ng, G. X. Wang, and H. K. Liu, J. Power Sources **162**, 1451 (2006).
[30] R. N. Reddy and R. G. Reddy, J. Power Sources **156**, 700 (2006).
[31] C. M. Huang, C. C. Hu, K. H. Chang, J. M. Li, and Y. F. Li, J. Electrochem. Soc. **156**, A667 (2009).
[32] Y. Jin, C. P. Yang, X. H. Rui, T. Cheng, and C. H. Chen, J. Power Sources **196**, 5623 (2011).
[33] Y. D. Li, S. X. Zhao, C. W. Nan, and B. H. Li, J. Alloys Compd. **509**, 957 (2011).
[34] Y. Cui, Z. L. Zhao, and R. S. Guo, J. Alloys Compd. **490**, 236 (2010).
[35] X. H. Rui, J. X. Zhu, D. Sim, C. Xu, Y. Zeng, H. H. Hng, T. M. Lim, and Q. Y. Yan, Nanoscale **3**, 4752 (2011).
[36] L. Q. Tao, J. T. Zai, K. X. Wang, Y. H. Wan, H. J. Zhang, C. Yu, Y. L. Xiao, and X. F. Qian, RSC Adv. **2**, 3410 (2012).
[37] M. M. Doeff, Y. Hu, F. McLarnon, and R. Kostecki, Electrochem. Solid-State Lett. **6**, A207 (2003).
[38] Y. Hu, M. M. Doeff, R. Kostecki, and R. Finones, J. Electrochem. Soc. **151**, A1279 (2004).
[39] C. T. Hsieh, C. T. Pai, Y. F. Chen, P. Y. Yu, and R. S. Juang, Electrochim. Acta **115**, 96 (2014).
[40] F. Mestre-Aizpurua, S. Hamelet, C. Masquelier, and M. R. Palacin, J. Power Sources **195**, 6897 (2010).
[41] T. Kurita, J. C. Lu, M. Yaegashi, Y. Yamada, S. Nishimura, T. Tanaka, T. Uzumaki, and A. Yamada, J. Power Sources **214**, 166 (2012).

DOI:10.1063/1674-0068/28/cjcp1502025